NMR-Derived Dynamic Aspects of N-Type Inactivation of a Kv Channel Suggest a Transient Interaction with the T1 Domain

Kent A. Baker,[‡] Christian Hilty,[§,||] Wolfgang Peti,[⊥,#] Alison Prince,[¶] Paul J. Pfaffinger,[¶] Gerhard Wider,[§] Kurt Wüthrich,[§,⊥] and Senyon Choe*[,‡]

Structural Biology Laboratory, The Salk Institute, La Jolla, California 92037, Institut für Molekularbiologie und Biophysik, ETH Zürich, 8093 Zürich, Switzerland, The Scripps Research Institute, La Jolla, California 92037, and Department of Neuroscience, Baylor College of Medicine, Houston, Texas 77030

Received August 17, 2005; Revised Manuscript Received November 21, 2005

ABSTRACT: Some eukaryotic voltage-gated K^+ (Kv) channels contain an N-terminal inactivation peptide (IP), which mediates a fast inactivation process that limits channel function during membrane depolarization and thus shapes the action potential. We obtained sequence-specific nuclear magnetic resonance (NMR) assignments for the polypeptide backbone of a tetrameric N-terminal fragment (amino acids 1−181) of the *Aplysia* Kv1.1 channel. Additional NMR measurements show that the tetramerization domain 1 (T1) has the same globular structure in solution as previously determined by crystallography and that the IP (residues 1−20) and the linker (residues 21−65) are in a flexibly disordered, predominantly extended conformation. A potential contact site between the T1 domain and the flexible tail (residues 1−65) has been identified on the basis of chemical-shift changes of individual T1 domain amino acids, which map to the T1 surface near the interface between adjacent subunits. Paramagnetic perturbation experiments further indicate that, in the ensemble of solution conformers, there is at least a small population of species with the IP localized in close proximity to the proposed interacting residues of the T1 tetramer. Electrophysiological measurements show that all three mutations in this pocket that we tested slow the rate of inactivation and speed up recovery, as predicted from the preinactivation site model. These results suggest that specific, short-lived transient interactions between the T1 domain and the IP or the linker segment may play a role in defining the regulatory kinetics of fast channel inactivation.

Cytoplasmic domains of voltage-gated K^+ (Kv)[1] channels regulate channel assembly, trafficking, and function and control cytoplasmic access to the ion-conduction pathway (*1*−*7*). Inactivation of Kv channels is a critical biological timing mechanism that limits the duration of channel activity in response to depolarization, as well as suppressing further channel activity for a period of time following depolarization. Thus, the ability to inactivate is an essential property of a variety of channels involved in shaping and regulating the excitability of the cell (*2*). A particular form of rapid inactivation of Kv channels, called N-type inactivation, is mediated by an inactivation peptide (IP) segment of approximately 20 amino acids located at the N-terminal end of the α subunits or certain associating β subunits. Results from experiments with free synthetic IPs, which restore inactivation to IP-free Kv channels (*3*, *8*, *9*), support the idea that a single IP can function by physically occluding the central ion pathway of open channels (*10*, *11*), independent of its covalent association with the channel.

Because of the presence of the bulky tetramerization domain 1 (T1) assembly located between the IP and the central IP-binding site (*12*−*14*) and because the central cavity of the T1 domain is not part of the ion-conduction pathway (*15*), it has been hypothesized that there must exist a pathway that allows the IP to move around the intervening T1 domain to reach its target site within the transmembrane (TM) pore of the channel and that the lateral "side-windows" formed between T1 and the TM domains most likely provide this route (*14*−*18*). This structural framework was confirmed by the recent crystal structure of rat Kv1.2 in complex with Kβ2 associated with the N-terminal membrane-distant side of the T1 domain (*19*). Given the narrowness of the lateral openings in the structure, it appears that the IP and the linker segment would have to be highly flexible, nonglobular structures to access the ion-conduction pathway of the TM pore domain.

Nuclear magnetic resonance (NMR) structures of isolated IPs display different protein conformations, from unstructured to ball-shaped (*20*, *21*). These observations indicate that the IP could either always be disordered and available to bind inside the channel after the pore opens or that the IP and the linker interact with other parts of the channel until they are

* To whom correspondence should be addressed. E-mail: choe@salk.edu. Telephone: (858) 453-4100. Fax: (858) 452-3683.
‡ The Salk Institute.
§ ETH Zürich.
|| Present address: Lawrence Berkeley National Laboratory, Berkeley, CA 94720.
⊥ The Scripps Research Institute.
Present address: Brown Medical School, Providence, RI 02912.
¶ Baylor College of Medicine.

[1] Abbreviation: T1, tetramerization domain 1; NMR, nuclear magnetic resonance; IP, inactivation peptide; Kv, voltage-gated potassium (K); TM, transmembrane; TROSY, transverse relaxation-optimized spectroscopy; aKv1.1N, N-terminal domain of *Aplysia* Kv1.1 channel; aKv1.1T1, T1 domain of *Aplysia* Kv1.1 channel; NOESY, nuclear Overhauser spectroscopy.

10.1021/bi0516430 CCC: $33.50
Published on Web 01/20/2006

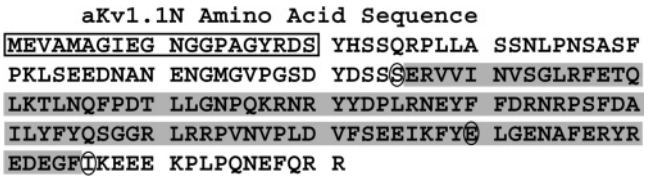

FIGURE 1: Amino acid sequence of aKv1.1N. The IP (amino acids 1−20) and T1 (amino acids 66−165) domains are indicated with open and shaded boxes, respectively. Amino acids differing from the wild-type sequence are R30A, R38A, C63S, and C65S, which were exchanged to prevent unwanted proteolysis and slow aggregation. The ovals indicate the three amino acids that were exchanged to cysteine for the purpose of MTSL labeling (see the text).

triggered to unfold. If the IP is always ready to bind, then the rate of inactivation will be largely driven by the availability of the binding site. Alternatively, if the IP and the linker remain preferentially bound to their residential "pocket", they may need to disengage and/or unfold to bind to their IP-binding site. To address the structural framework of the IP and the linker segment in relation to the T1 domain, we have carried out a NMR investigation of the N-terminal domain of the *Aplysia* Kv1.1 voltage-gated potassium channel, aKv1.1N, which contains residues 1−181 (Figure 1), ending approximately 5 amino acids prior to the first TM helix, S1 (*19*). The aKv1.1N protein is a soluble tetrameric assembly with a molecular weight of approximately 84 kD. Transverse relaxation-optimized spectroscopy (TROSY)-based NMR methods (*22*) on high-field instruments and the use of uniform and amino acid-specific stable-isotope labeling allowed for the sequence-specific resonance assignment as the basis for structural characterization. Additionally, the resonance assignment of the T1 domain tetramer of residues 66−173, aKv1.1T1, was also completed. Finally, paramagnetic probes attached at membrane-proximal, central, or membrane-distant regions of the T1 domain were used to estimate the extent of transient proximity of the IP and the linker with respect to different surface areas of the T1 domain.

MATERIALS AND METHODS

Protein Preparation. Two expression constructs were used on the basis of the Shaker Kv1.1 gene from *Aplysia* (M95914). The first construct used the coding sequence for amino acids 66−173 of the gene in the vector pET-24a and included a noncleavable C-terminal 6×His tag (*13*). The second construct used the coding sequence for amino acids 1−181 in a customized pET-28 and included a thrombin cleavable N-terminal 8×His tag, leaving four additional amino acids (Gly-Ser-His-Gly) attached at the N terminus after cleavage. Four amino acid substitutions (R30A, R38A, C63S, and C65S) were introduced in the native sequence of aKv1.1N to help improve protein stability. These mutations, when introduced into the intact channel, do not affect the inactivation properties of the intact channel. Proteins were expressed in BL-21(DE3) *Escherichia coli* and purified in a single step by metal-affinity chromatography.

Two expression methods were used to produce uniformly isotope-labeled protein. The first is an adaptation of the method published by Marley et al. (*23*). BL21(DE3) *E. coli* were transformed with the desired expression construct, grown at 37 °C in LB to $OD_{600\ nm} \approx 0.7$, then spun down, rinsed with PBS, and resuspended in minimal media containing the isotope label. A volume ratio of 4:1 LB/minimal media was used to produce a high-density sample prior to induction. After 1 h, bacteria were induced with 0.5 mM IPTG for 5 h at 37 °C. This method allowed for high levels of protein expression but reduced isotope incorporation to approximately 80%. Proteins with ^{15}N selectively labeled amino acids were produced using the auxotrophic DL-39 *E. coli* strain (*24*). Expression was similar to the above but with defined media containing a single ^{15}N-labeled amino acid replacing the minimal media (*25*). Samples of aKv1.1N were produced with aspartic acid, leucine, phenylalanine, and valine selectively labeled. Uniformly labeled samples were also produced using Celtone isotope-labeling media (Spectra Stable Isotopes) to increase the level of isotope incorporation. Bacteria were grown at 37 °C in Celtone to an $OD_{600\ nm} \approx 0.7$ and then induced with 0.5 mM IPTG for 5 h.

After growth and induction, the cells were lysed, the resulting lysate was centrifuged to clear cellular debris and applied to metal-affinity resin. The resin was thoroughly rinsed, and then the purified protein was eluted with 0.25 M imidazole. Samples with cleavable His tags were treated with a 1:1500 mass ratio of thrombin overnight prior to final processing. Purified protein samples were exchanged into 20 mM sodium phosphate at pH 7.0, 50 mM NaCl, and 5% D_2O and concentrated by ultrafiltration, unless otherwise noted. Sample concentrations ranged from 0.7 to 1.5 mM monomeric protein.

NMR Spectroscopy. A 3D TROSY-HNCA spectrum was recorded with [70% ^2H,u-^{13}C,^{15}N]-aKv1.1T1 on a Bruker Avance 800 spectrometer with 40 transients per increment (*26*). Time-domain data size was 32 (t_1) × 41 (t_2) × 512 (t_3) complex points, and evolution times $t_{1,max}(^{15}N) = 13.1$ ms, $t_{2,max}(^{13}C) = 7.8$ ms, and $t_{3,max}(^1H) = 53.3$ ms were used. Of the same sample, 3D [^{13}C]-*ct*-TROSY-HNCA (*27*) and 3D TROSY-HNCACB (*28*) spectra were recorded on a Bruker Avance 900 spectrometer, with the former having time-domain data size 32 (t_1) × 150 (t_2) × 512 (t_3) complex points, evolution times $t_{1,max}(^{15}N) = 11.0$ ms, $t_{2,max}(^{13}C) = 23.4$ ms, and $t_{3,max}(^1H) = 40.6$ ms, and 16 transients per increment and the latter having time-domain data size 32 (t_1) × 80 (t_2) × 1024 (t_3) complex points, evolution times $t_{1,max}(^{15}N) = 12.5$ ms, $t_{2,max}(^{13}C) = 6.2$ ms, and $t_{3,max}(^1H) = 81.2$ ms, and 32 transients per increment. On a 500 MHz spectrometer with a cryogenic probehead, a (H)N(COCA)-NH spectrum (*29*) of [u-^2H,^{13}C,^{15}N]-aKv1.1N was measured with a time-domain data size of 35 (t_1) × 64 (t_2) × 512 (t_3) complex points. Evolution times were $t_{1,max}(^{15}N) = 21$ ms, $t_{2,max}(^{15}N) = 39$ ms, and $t_{3,max}(^1H) = 79$ ms, and 8 transients per increment were acquired. [^1H,^1H]-nuclear Overhauser spectroscopy (NOESY)-[^{15}N,^1H]-TROSY spectra (30) were recorded for [70% ^2H,u-^{15}N]-aKv1.1T1, with nuclear Overhauser effect (NOE) mixing times of 60 and 120 ms. The 60-ms spectrum was recorded on a Bruker Avance 800 spectrometer with 150 (t_1) × 37 (t_2) × 1024 (t_3) complex points, $t_{1,max}(^1H) = 15.6$ ms, $t_{2,max}(^{15}N) = 15.2$ ms, and $t_{3,max}(^1H) = 106$ ms, and 16 transients per increment. The 120-ms spectrum was recorded on a Bruker Avance 900 spectrometer with 128 (t_1) × 32 (t_2) × 1024 (t_3) complex points, $t_{1,max}(^1H) = 11.9$ ms, $t_{2,max}(^{15}N) = 11.7$ ms, and $t_{3,max}(^1H) = 95.0$ ms, and 16 transients per increment. For

[u-^{2}H,^{13}C,^{15}N]-aKv1.1N, a [^{1}H,^{1}H]-NOESY-[^{15}N,^{1}H]-TROSY spectrum was recorded on a Bruker Avance 900 MHz spectrometer with a NOE mixing time of 200 ms, time-domain data size of 138 (t_1) × 35 (t_2) × 1024 (t_3) complex points, $t_{1,max}$(^{1}H) = 12.8 ms, $t_{2,max}$(^{15}N) = 12.0 ms, and $t_{3,max}$-(^{1}H)= 97.5 ms, and 16 transients per increment. With the same sample, a 900 MHz 3D TROSY-HNCA experiment was recorded with time-domain data size of 32 (t_1) × 32 (t_2) × 512 (t_3) complex points, $t_{1,max}$(^{15}N) = 12.6 ms, $t_{2,max}$-(^{13}C) = 5.0 ms, and $t_{3,max}$(^{1}H)= 43.9 ms, and 64 transients per increment. The 800 and 900 MHz spectrometers were equipped with three high-power radio-frequency channels for the ^{1}H, ^{13}C, and ^{15}N pulses, low power 20 W amplifiers for ^{2}H-decoupling, and ^{1}H-{^{13}C,^{15}N} triple-resonance probes with actively shielded gradients. TROSY-based ^{15}N{^{1}H}-NOE experiments (*31*) were measured for [70% ^{2}H,u-^{13}C, ^{15}N]-aKv1.1T1 and [70% ^{2}H,u-^{13}C,^{15}N]-aKv1.1N on a Bruker DRX 500 spectrometer equipped with four high-power radio-frequency channels for generating ^{1}H, ^{2}H, ^{13}C, and ^{15}N pulses and a ^{1}H-{^{13}C,^{15}N} triple-resonance cryogenic probe with an actively shielded *z* gradient. Time-domain data size was 125 (t_1) × 1024 (t_2) complex points for both the reference spectrum and the NOE experiment, which were measured in an interleaved manner. Evolution times were $t_{1,max}$(^{15}N) = 74.7 ms and $t_{2,max}$(^{1}H) = 128 ms, and 20 transients per increment were acquired. Two-dimensional [^{15}N,^{1}H]-TROSY spectra (*32*) of the selectively labeled [[^{15}N]-Leu]-aKv1.1T1, [[^{15}N]-Phe]-aKv1.1T1, and [[^{15}N]-Val]-aKv1.1T1 samples, as well as of [70% ^{2}H,u-^{15}N]-aKv1.1N samples used for functional studies, were recorded with similar experimental parameters. All NMR experiments were performed at 37 °C.

The time-domain data were processed either with Bruker XWINNMR software or with PROSA (*33*), applying cosine window functions in all dimensions and using zero-filling to twice the recorded data size. Spectral analysis was performed using XEASY (*34*) and CARA (R. Keller et al., unpublished results). Chemical shifts were referenced to 2,2-dimethyl-2-silapentane-5-sulfonate sodium salt (DSS) (*35*).

Paramagnetic Perturbation Analysis by NMR. Paramagnetic perturbation analysis and the preparation of the MTSL samples followed methods described by Battiste and Wagner (*36*, *37*). Single cysteines were introduced (or reintroduced in the case of amino acid 65) one by one at positions 65, 150, and 166 in aKv1.1N. The resulting variant aKv1.1N proteins were buffered in 20 mM sodium phosphate at pH 7.0, 100 mM NaCl, and 1 mM [tris(2-carboxyethyl)]-phosphine (TCEP). The protein was then diluted in a 10-fold molar excess of MTSL (Toronto Research Chemicals, Inc.). After overnight incubation at room temperature, the excess MTSL was removed by dialysis. The protein was then concentrated by ultrafiltration for the collection of [^{15}N,^{1}H]-TROSY spectra. The MTSL was then reduced by the addition of 5 mM ascorbic acid to each sample, after which another [^{15}N,^{1}H]-TROSY spectrum was collected. Within each pair of spectra, individual peak amplitudes were measured and compared. In each of the three experiments, we observed the entire range of possible effects from the spin label, with peaks that were broadened beyond detectability because of proximity and others that were completely unperturbed. Amplitudes were used instead of peak integrals because of peak crowding. Because of the 4-fold symmetric assembly of the T1 tetramer, discrete distances could not be calculated between the spin label and any given amino acid. Instead, ratios of peak amplitudes were used to derive position information relative to the different probe locations. As an internal calibration control, the perturbation for three amino acids within 10 Å of each probe was calculated.

Electrophysiology. Mutations were introduced into a wild-type aKv1.1 construct and verified by sequencing. Constructs were linearized and cRNA-transcribed, injected into *Xenopus* oocytes, and recorded as described previously (*15*), except that recordings were performed with 98 mM K_o to suppress C-type inactivation, which occurs rapidly following N-type inactivation in low external K_o. A total of 4−6 separate recordings were performed for each condition. N-type inactivation and suppression of C-type inactivation were confirmed in these recordings by examining the tail currents during recovery from inactivation. Tails showed a clear N-shape and time course, matching the recovery time course as predicted for N-type inactivation. A small amount of C-type inactivation of less than 5% may occur during these recordings, but the much slower recovery from C-type inactivation, with a time constant ∼ 3 s, allowed us to separately fit the >95% N-type recovery. To estimate the energetic effects of these mutations, we calculated an apparent binding affinity, K_A, as the ratio of the inactivation time constant at +50 mV to the recovery time constant at −100 mV. We then calculated an apparent energy cost for the mutations as RT ln(K_A(mutant)/K_A(WT)).

RESULTS AND DISCUSSION

Two-dimensional [^{15}N, ^{1}H]-TROSY correlation spectra of both aKv1.1T1 and aKv1.1N (parts A and B of Figure 2) showed single resonances for each amino acid of the monomer sequence, indicating that both proteins are homogeneous, symmetric tetramers. The line widths for aKv1.1N of approximately 42 Hz for ^{1}H and 27 Hz for ^{15}N are consistent with the large particle size of the tetramer. For the sequential assignment, we used a combination of 3D TROSY-HNCA, 3D constant-time TROSY-HNCA, and 3D ^{15}N-resolved [^{1}H,^{1}H]-NOESY-[^{15}N,^{1}H]-TROSY spectra of the uniformly ^{2}H,^{13}C,^{15}N-labeled proteins (parts C and D of Figure 2) and 2D [^{15}N,^{1}H]-TROSY correlation spectra of the proteins with residue-specific ^{15}N-labeling. For the assignment of the IP and linker segments of aKv1.1N, which have very limited ^{1}H chemical-shift dispersion, 3D (H)N(COCA)-NH spectra (*29*) provided additional sequential connectivities. The assignment of the polypeptide backbone is nearly complete, except for the residues 18−35. The chemical-shift lists have been deposited in the BMRB (accession number 6879).

The C^{α} chemical-shift deviations from the random-coil values in aKv1.1N are in good agreement with predictions from the secondary structure of the T1 tetramer crystal structure (Figure 3). The ^{15}N-resolved [^{1}H,^{1}H]-NOESY spectra of aKv1.1N also contain most of the long-range main-chain cross-peaks expected from the interatomic distances calculated from the T1 tetramer structure (PDB ID 1T1D), showing that the T1 domain structure in aKv1.1N coincides with that of the previously determined crystal structure. From a comparison of the [^{15}N,^{1}H]-TROSY correlation spectra of aKv1.1N and aKv1.1T1, it is apparent that there is close coincidence of the T1 domain in the two constructs and that

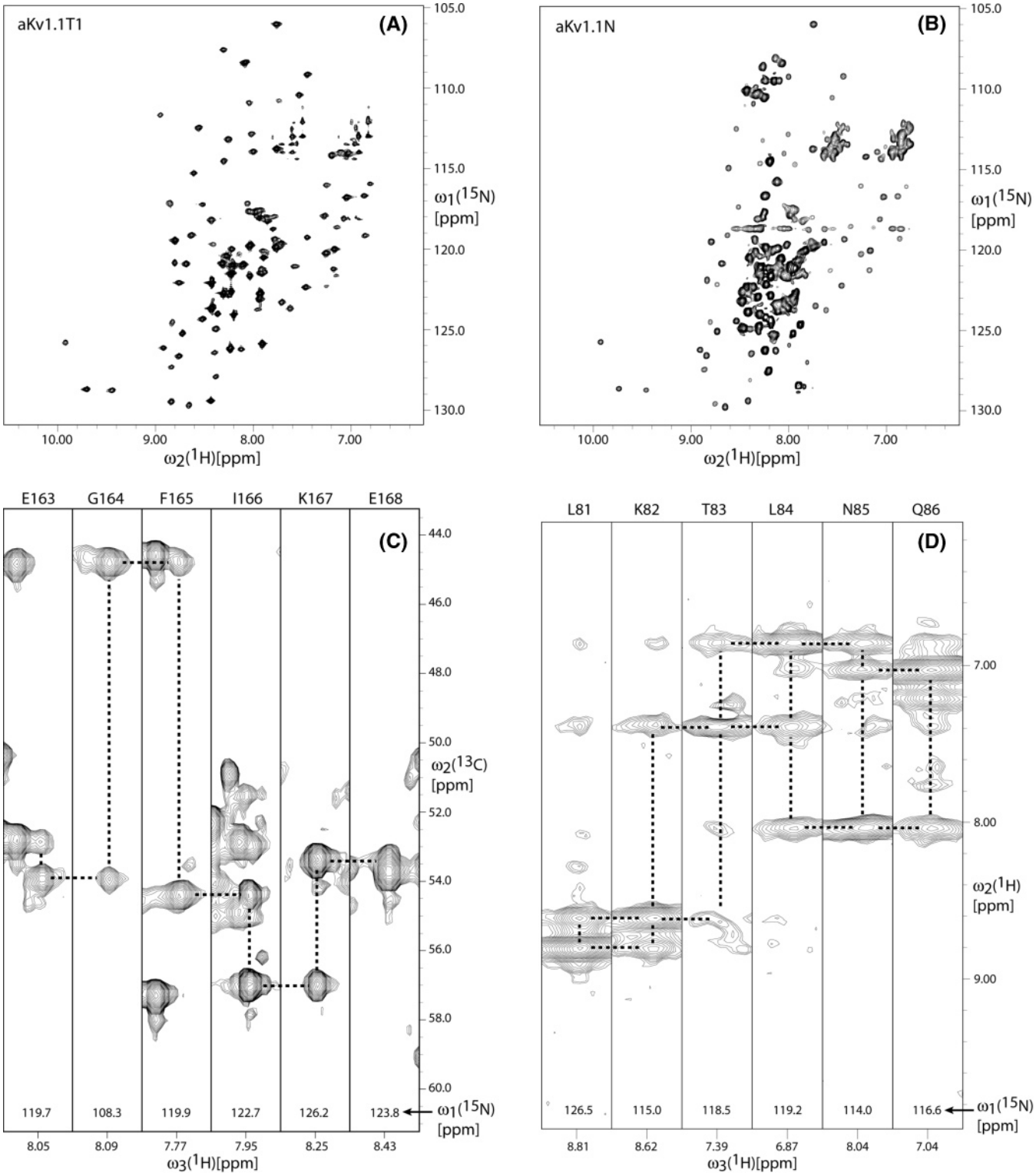

FIGURE 2: (A and B) [^{15}N,^{1}H]-TROSY correlation spectra for aKv1.1T1 and aKv1.1N, respectively. (C) Strips for the amino acids 163−168 from a 3D TROSY-HNCA spectrum of aKv1.1N. (D) Strips for the amino acids 81−86 from a [^{1}H,^{1}H]-NOESY-[^{15}N,^{1}H]-TROSY spectrum of aKv1.1N. Sequential relationships in C and D are represented by dashed lines. The spectra A−C were measured at 900 MHz, and the spectrum D was measured at 800 MHz, with a ~1 mM monomer concentration at pH 7.0 and 37 °C.

the additional resonances of the IP and the linker in aKv1.1N have narrower line widths and higher intensities than the T1 resonances, indicating shorter correlation times for these residues. The IP and linker also have only small deviations from the random-coil chemical shifts and show no long-range NOEs, indicating that they do not have a globule-like structure.

These indications of variable mobility along the amino acid sequence of aKv1.1N are confirmed by heteronuclear ^{15}N{^{1}H}-NOE measurements (Figure 3B). The T1 domain shows positive ^{15}N{^{1}H}-NOEs, typical of large globular proteins, whereas the IP and the linker show negative NOE values that indicate intramolecular mobility of these polypeptide segments within the large structure of the aKv1.1N

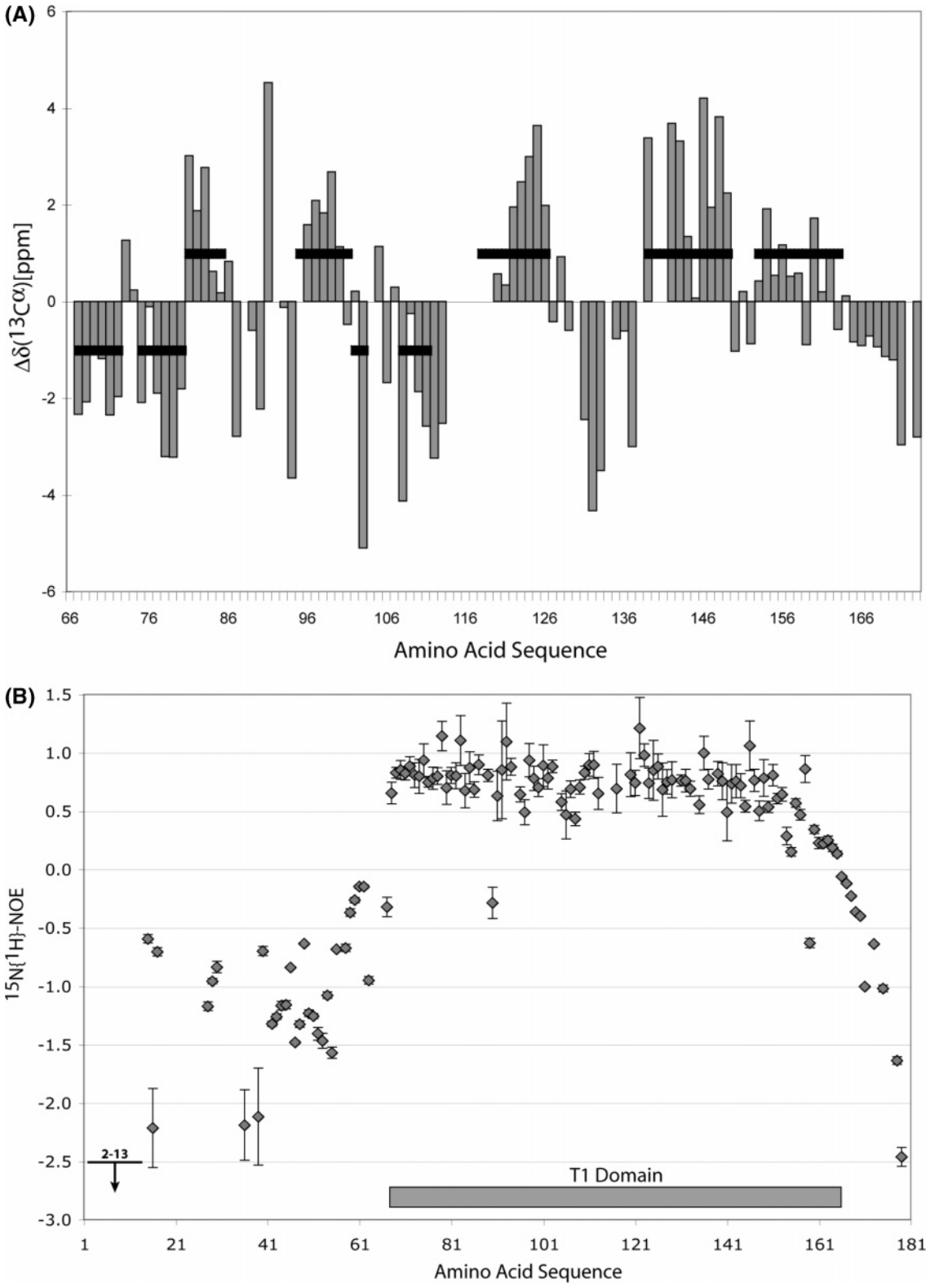

FIGURE 3: (A) Chemical-shift deviations from the random-coil values for the C^{α} resonances of the T1 domain from aKv1.1N. The "Restricted Set of Protein Chemical Shifts, BMRB 2002" was used as the reference random-coil chemical shifts. The locations of secondary-structure elements identified in the crystal structure of T1 (PDB ID 1T1D) are indicated by horizontal black bars at +1 for α helices, and at −1 for β sheets. (B) Backbone steady-state $^{15}N\{^{1}H\}$-NOE values for aKv1.1N. Positive and negative values indicate rigid and dynamic regions, respectively. For the amino acids 2−13 (indicated by an arrow) and 180−181 (not shown), only an upper limit of −2.5 could be determined (see the text). The location of the T1 domain is indicated at the bottom by a gray box.

tetramer. Only upper limits of −2.5 could be determined for the chain termini and the amino acids 2−13 and 180−181, mainly because of spectral overlap of the corresponding signals in the random-coil chemical-shift region.

There are a small number of sizable chemical-shift differences for corresponding amino acids between aKv1.1T1 and aKv1.1N (Figure 4A). Other than the N and C termini of T1, for which differences are expected because of the

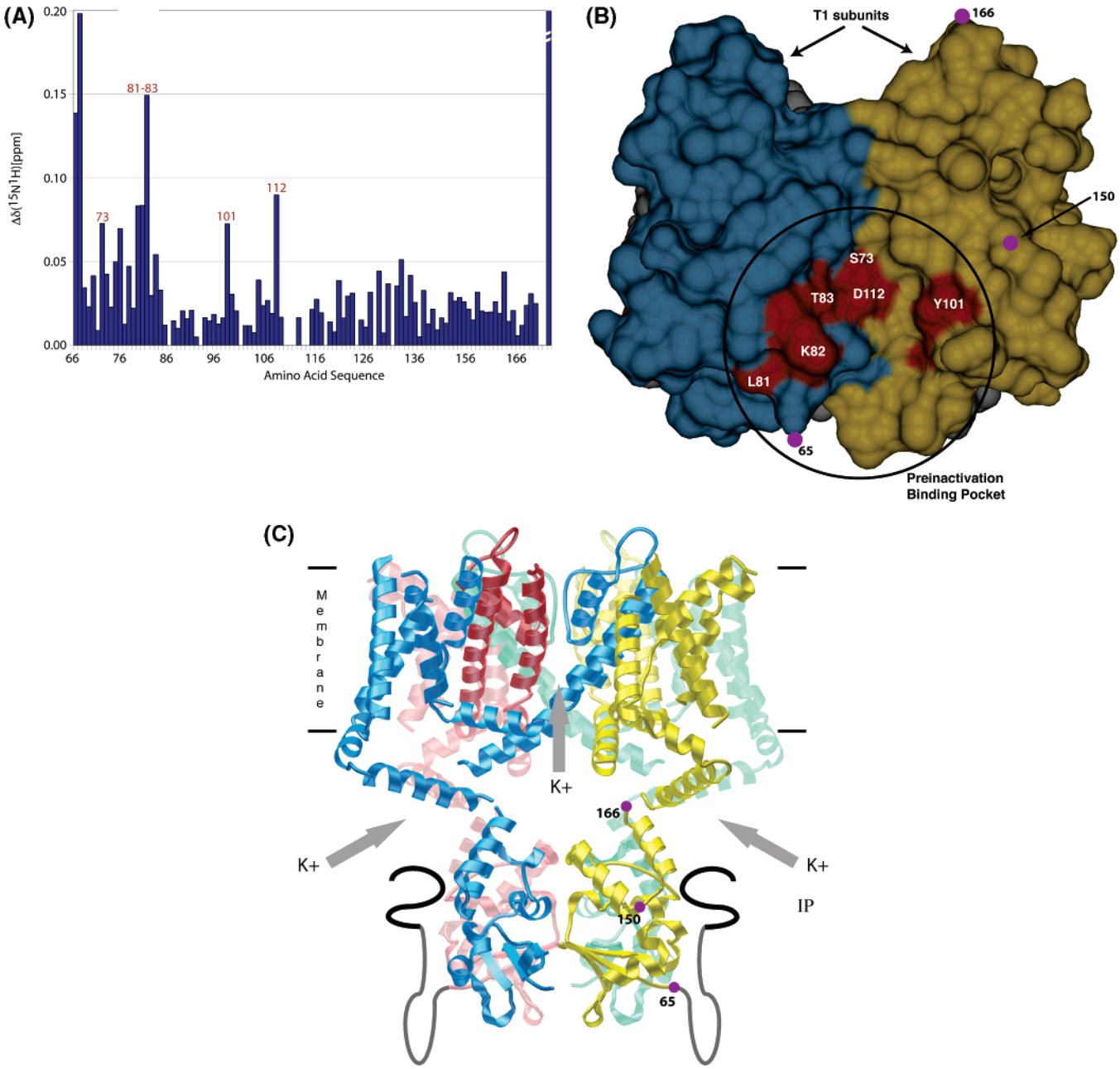

FIGURE 4: (A) Normalized chemical-shift differences $[\Delta\delta(^{15}N,^{1}H) = [\Delta\delta(^{1}H)^2 + (0.2\Delta\delta(^{15}N))^2]^{1/2}]$ measured between corresponding residues in $[^{15}N,^{1}H]$-TROSY spectra of aKv1.1T1 and aKv1.1N. Shifts greater than 0.07 ppm of nonterminal residues are labeled with the sequence positions 73, 81−83, 101, and 112. (B) Residues with $\Delta\delta(^{15}N,^{1}H) > 0.07$ ppm in A are mapped in red on the T1 tetramer surface. Adjacent T1 monomers are shaded blue and gold. Positions used for MTSL labeling are marked with magenta circles. (C) Molecular architecture diagram of a eukaryotic potassium channel. The TM and T1 domains from the rat Kv1.2 structure (PDB ID 2A79) are shown in red, green, blue, and yellow. The linkers of residues 21−65 and the IP are represented as gray and black lines, respectively. The K^+ conduction pathway is indicated with arrows. The positions used for MTSL labeling are indicated by magenta dots. For clarity, only two diagonally related linkers and IPs are shown.

changes in the chemical structure, the six amino acids, S73, L81, K82, T83, Y101, and D112, show pronounced changes. A surface rendering of the T1 tetramer (Figure 4B) shows that, although these residues are quite distant from each other in the sequence, they are all located in close proximity on the surface at a cleft between two adjacent monomers of the T1 tetramer. This cleft is large enough (approximately 12 Å deep and 20 Å long) to accommodate a part of the linker. This surface area of the T1 tetramer is thus a prime candidate for being a transient binding site for the IP, linker, or both.

To determine whether environmental changes that the cytoplasmic domain may experience during the selective ion flux of the active channel regulate these interactions, we measured changes of the chemical shifts in response to the salt concentration. There are only small chemical-shift changes induced in aKv1.1N by increasing the salt concentration from 50 to 400 mM with NaCl or KCl (data not shown). More importantly, there is also no significant cation-specific difference between NaCl and KCl at equal concentrations. These results indicate that aKv1.1N does not undergo any detectable conformational changes or "disengagement" of the IP or linker in response to static cation concentration changes. Instead, such changes can possibly be caused by a protein conformational change propagating

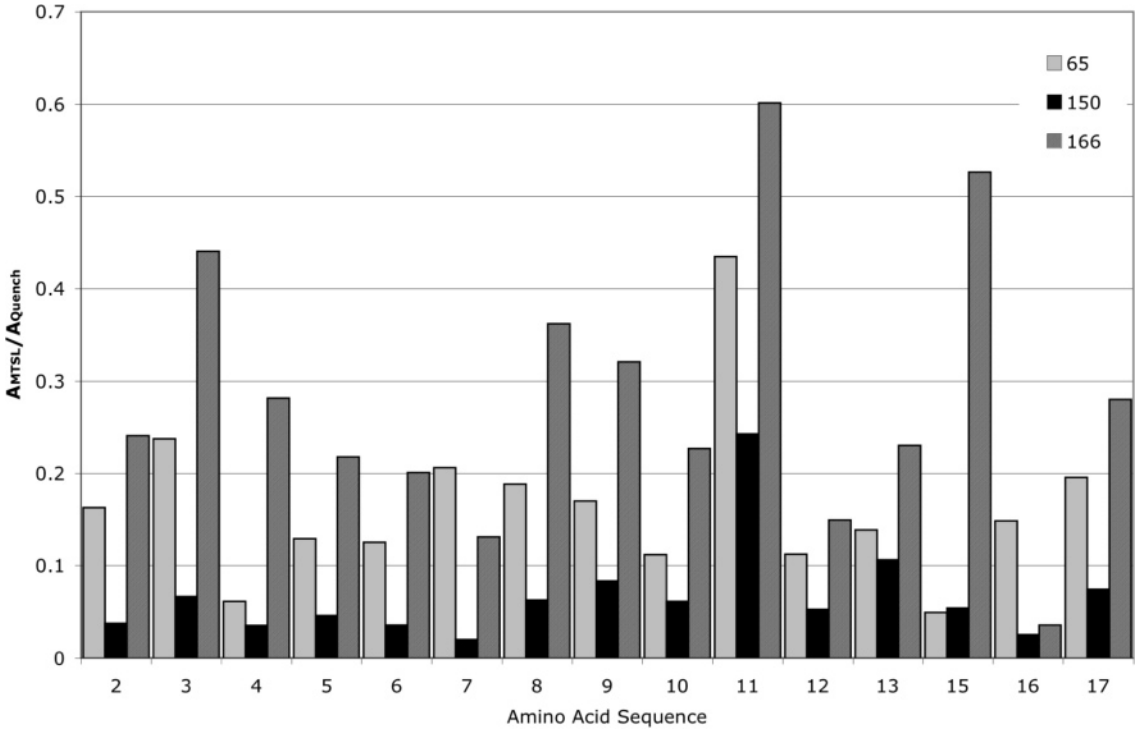

FIGURE 5: Plots of the ratio of the amplitudes of corresponding [^{15}N-^{1}H] correlation peaks in Kv1.1N in the presence of a MTSL spin label (A_{MTSL}) and after ascorbic acid reduction of the MTSL (A_{quench}) for the N-terminal 17 amino acids of the IP. The broadening arising from the spin label at each of the three positions 65, 150, and 166 (Figure 4) is represented in light gray, black, and dark gray, respectively.

from the voltage-sensing module of the activated channel or by potassium-current-induced electrostatic effects.

To better characterize the spatial relationship between the IP, linker, and T1 domain, we covalently attached an NMR broadening agent, the nitroxide spin label 1-oxyl-2,2,5,5-tetramethyl-methanethiosulfonate (MTSL), to cysteines engineered into aKv1.1N separately at the amino acids 65, 150, and 166 (indicated in parts B and C of Figure 4). Positions 65 and 166 are immediately adjacent to the N and C termini of the T1 domain. Position 150 is approximately halfway between residues 65 and 166, facing outward. MTSL enhances the relaxation of the surrounding resonances, resulting in a loss of peak amplitude, in a distance-dependent manner (*36*, *37*). [^{15}N,^{1}H]-TROSY spectra of these proteins were compared with control spectra to measure the reduction in the peak amplitude (Figure 5). Figure 5 shows ratios of amplitudes for corresponding peaks in the presence and absence of the spin label (see the Materials and Methods). Placing the probe at position 150 causes the most substantial loss in the [^{15}N,^{1}H]-TROSY spectral signals for residues on the IP. Placing the probe at position 65 results in more signal loss for the IP than when placed at position 166. Amino acids in the linker become progressively more perturbed by the 65 probe as they approach the junction with T1, as would be expected (data not shown).

As a reference for our analysis of the MTSL labeling, the perturbation of three amino acids within 10 Å of each probe was calculated. Labeling at position 65 broadened peaks from amino acids 62, 63, and 79 on average to the extent of 91%. Labeling at position 150 broadened peaks from amino acids 89, 90, and 152 on average 97%. Labeling at position 166 broadened peaks from amino acids 139, 163, and 164 on average 97%. The spin-label experiments thus suggest that the linker is primarily located near the bottom of T1 (near amino acid 66), whereas the IP appears to be distributed over a wider range of conformational space with respect to T1 (modeled in Figure 4C).

The structural model predicts that binding of the IP and linker to the T1 domain will reduce the entropic costs associated with IP entry and stability in the pore-binding site. To test this model directly, we introduced mutations into the binding site residues K82, D112, and Y101 (Figure 4A). These residues are in close proximity in the three-dimensional structure (Figure 4B). The mutants were characterized for their effects on channel inactivation properties. To isolate N-type inactivation from C-type inactivation, recording was performed at an elevated external K^+ concentration. Figure 6A compares the inactivation kinetics of wild-type (WT) channels to those with the K82A mutation in response to a 1 s voltage step to +50 mV. In comparison to WT channels, K82A slows the kinetics of inactivation and results in a larger level of sustained, noninactivated current. Upon repolarization, the K82A mutant produces a long transient tail current because of the closing of the noninactivated channels and the rapid recovery of IP-blocked channels that transits through the open state before closing. The WT current also shows a tail current characteristic of recovery from N-type inactivation, but this current is smaller and slower than for K82A.

In addition to slowing inactivation kinetics, the recovery from inactivation is greatly accelerated by the K82A mutation (Figure 6B). Currents were inactivated during a 1 s pulse to +50 mV and allowed to recover for varying times at −100 mV before retesting with a second pulse to +50 mV. The more rapid recovery of the second-pulse amplitude for K82A is clearly apparent. Figure 6C plots the recovery kinetics at −100 mV for WT and the K82A, D112A, and Y101A mutants. All mutations to this binding site accelerate the

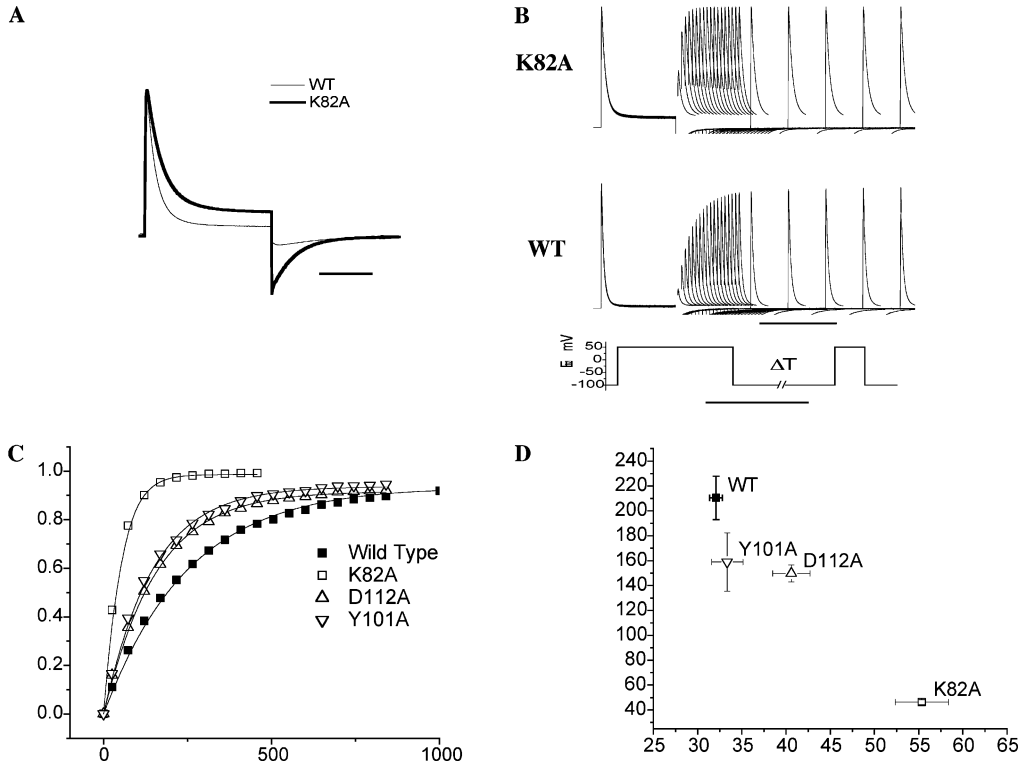

FIGURE 6: Electrophysiological measurements of N-type inactivation by the interaction of IP and linker with the T1 domain. Alanine mutations to K82, D112, and Y101 were characterized. Currents were recorded in *Xenopus* oocytes following cRNA injections. (A) Currents from K82A channels were compared to the wild type in response to a voltage step from −100 to +50 mV and back. The K82A mutation delays N-type inactivation and results in a large fraction of noninactivating current as seen by the large tail current. The scalebar is 200 ms. (B) Recovery of channels from N-type inactivation is accelerated by the K82A mutation as characterized by the more rapid recovery of the current amplitude in a second pulse to +50 mV following variable time at −100 mV. The scalebar for time is 1 s. (C) Summary graph showing the accelerated recovery from inactivation for K82A, D112A, and Y101A. The *x* axis is for recovery time in milliseconds. The *y* axis is for normalized current. (D) Summary plot showing that the mutations proportionally slow the rate of inactivation and speed up the recovery from inactivation, suggesting a mechanism with a common energetic basis of action for this site. Linear regression between these points fits with a correlation coefficient of 0.96. The *x* axis is for inactivation Tau in milliseconds. The *y* axis is for recovery Tau in milliseconds.

recovery from N-type inactivation, with K82A having the largest effect.

If we compare the relative effects of these mutations on the time constant to inactivate versus the time constant to recover from inactivation, we can see that there is a clear linear relationship between these parameters: greater slowing of inactivation produces greater acceleration of recovery with a correlation coefficient of 0.96. These results provide clear evidence for a significant functional role of this site in the regulation of channel inactivation and recovery kinetics. The combination of slower inactivation and more rapid recovery of K82A are in line with the higher levels of sustained current seen in Figure 6A. The different quantitative effects of the individual mutations on inactivation are likely due to different energetic effects on the binding affinity of the IP and chain to this site. Taking the ratio of time constants of inactivation to recovery as an approximate measure of the binding affinity, we estimate the following energetic costs: K82A, ~5 kJ/mol; D112A, ~1.4 kJ/mol; and Y101A, ~0.7 kJ/mol. The central location of K82 in the preinactivation-binding pocket, where it is flanked by amino acids 81 and 83 (Figure 4B), which also exhibited chemical-shift changes in the NMR experiments, provides a rationale for the observation that the amino acid replacement in this position has an outstandingly large effect.

In the native channel, the T1 domain constrains access of the N-terminal IP to the pore-lining cavity of the channel. Overall, the present NMR characterization of the isolated tetrameric assembly of the N-terminal 181-amino acid fragment of the *Aplysia* Shaker potassium channel shows that the T1 domain forms a central rigid scaffold, similar to that of the previous crystal structure, around which the disordered and flexible IP and its linker operate. The narrowness of this pathway and the length of the IP and linker implicate that the entropic loss of the IP being stretched in an extended conformation into the channel cavity must be compensated by the overall free-energy change produced by the binding of the IP. A tightly folded IP or linker would slow inactivation because of the high energetic cost of unfolding. Therefore, little energy is required for the IP to reach its site of action.

The nonuniform flexibility across the IP and its linker (Figure 3B) would be consistent with the hypothesis that the presence of a putative preinactivation binding pocket on the surface of T1 may help to reduce the entropic costs of constraining the flexible IP in the tortuous pathway to the IP-binding site within the TM pore domain (*3*). Furthermore, within the ensemble of IP/linker structures, only a small fraction needs to be bound to T1 at any one time, because only a single IP is sufficient to block the tetrameric channel (*11*). The experimental data collected in solution suggests that the IP/linker occupies the pocket on the T1 domain surface, suggesting that this interaction might serve in orienting the IP and thus potentially accelerate the process

of inactivation. If the IP is appropriately positioned by the interaction with T1 and poised to be drawn into the pore of the channel by the flux of positively charged potassium ions, this may facilitate more rapid IP binding than by slow random diffusion (*38*, *39*). Our results of the largest broadening effects of the IP by MTSL attached centrally about the periphery of the T1 domain are thus consistent with the view that the putative preinactivation binding pocket will form the energetic conduit to release the linker to undergo a conformational change. IP/linkers bound in this location can account for extra density observed in the low resolution electron microscopy structure of the full-length channel (*14*). This preinactivation binding of the IP and linker is in dynamic equilibrium with the fully extended conformation required for inactivation for which voltage-gated channel activation can trigger conversion.

In this study, we provide direct experimental evidence to make two conclusions that help explain the mechanism of inactivation. On one hand, we directly determine that the IP and linker are structurally flexible. On the other hand, nonuniform flexibility across the IP and linker segments and a likely site for interaction on the T1 domain exterior suggest that such transient interaction may help reduce the entropic costs of the IP action. Further support for this model from functional mutagenesis on the T1 domain show that certain mutations to putative surface-exposed residues modulate inactivation kinetics, possibly by disrupting a preinactivation site that docks the linker near the pore opening to inactivate the channel (*3*, *18*). The N-terminal tip of the IP has been previously shown to interact deep within the water-filled cavity region of the channel pore during inactivation (*3*); therefore, the energetics of conformational change and binding of the IP will play two opposite roles in this inactivation process. In our hypothesis, the IP remains preferentially positioned in its preinactivated state and undergoes conformational change only after the channel becomes activated.

To understand more about how the T1 domain is functionally coupled to the remainder of the channel, we will need further information on the flexibility of the linkages between the T1 and TM domains and on whether specific interaction occurs between these two regions of the channel during function. With nearly complete peak assignments available for the aKv1.1N, molecular interaction surfaces of aKv1.1N with other parts of the channel or other cytoplasmic proteins can now be traced if they can be formed as part of a larger covalent complex. The combination of specific structural and functional data on these interactions will be instrumental to characterize further the kinetic mechanisms underlying the regulation of channel activation and inactivation by cytoplasmic domains.

ACKNOWLEDGMENT

The authors thank members of the Choe and Wüthrich laboratories for critical comments and discussion. K. B. acknowledges fellowship support from the American Heart Association. This work was supported by the NIH (to S. C.) and by the Swiss National Science Foundation and the ETH Zürich through the NCRR "Structural Biology" Program (to K. W.).

REFERENCES

1. Gonzalez, C., Rosenman, E., Bezanilla, F., Alvarez, O., and LaTorre, R. (2001) Periodic perturbations in Shaker K^+ channel gating kinetics by deletions in the S3−S4 linker, *Proc. Natl. Acad. Sci. U.S.A. 98*, 9617−9623.
2. Hille, B. (2001) *Ion Channels of Excitable Membranes*, 3rd ed., Sinauer Associates, Sunderland, MA.
3. Zhou, M., Morais-Cabral, J., Mann, S., and MacKinnon, R. (2001) Potassium channel receptor site for the inactivation gate and quarternary amine inhibitors, *Nature 411*, 657−661.
4. Yellen, G. (2002) The voltage-gated potassium channels and their relatives, *Nature 419*, 35−42.
5. Gu, C., Jan, Y. N., and Jan. L. Y. (2003) A conserved domain in axonal targeting of Kv1 (Shaker) voltage-gated potassium channels, *Science 301*, 646−649.
6. Miller, C. (2003) A charged view of voltage-gated ion channels, *Nat. Struct. Biol. 10*, 422−424.
7. Roosild, T. P., Le, K. T., and Choe. S. (2004) Cytoplasmic gatekeepers of potassium channel flux: A structural perspective, *Trends Biochem. Sci. 29*, 39−45.
8. Hoshi, T., Zagotta, W. N., and Aldrich, R. W. (1990) Biophysical and molecular mechanisms of Shaker potassium channel inactivation, *Science 250*, 533−538.
9. Zagotta, W. N., Hoshi, T., and Aldrich, R. W. (1990) Restoration of inactivation in mutants of Shaker potassium channels by a peptide derived from ShB, *Science 250*, 568−571.
10. Bezanilla, F., and Armstrong C. M. (1972) Negative conductance caused by entry of sodium and cesium ions into the potassium channels of squid axons, *J. Gen. Physiol. 60*, 588−608.
11. MacKinnon, R., Aldrich, R., and Lee, A. W. (1993) Functional stoichiometry of Shaker potassium channel inactivation, *Science 262*, 757−759.
12. Kreusch, A., Pfaffinger, P., Stevens, C. F., and Choe, S. (1998) Crystal structure of the tetramerization domain of the Shaker potassium channel, *Nature 392*, 945−948.
13. Bixby, K., Nanao, M., Shen, V., Kreusch, A., Bellamy, H., Pfaffinger, P., and Choe, S. (1999) Zn^{2+}-mediated and molecular determinants of tetramerization in Kv channels, *Nat. Struct. Biol. 6*, 38−43.
14. Sokolova, O., Kolmakova-Partensky, L., and Grigorieff, N. (2001) Three-dimensional structure of a voltage-gated potassium channel at 2.5 nm resolution, *Structure 9*, 215−220.
15. Cushman, S. J., Nanao, M. H., Kunjilwaar, K., Jahng, A. W., DeRubeis, D., Choe, S., and Pfaffinger, P. J. (2000) Voltage-dependent activation of potassium channels is coupled to T1 domain structure, *Nat. Struct. Biol. 7*, 403−407.
16. Choe, S., Kreusch, A., and Pfaffinger, P. J. (1999) Towards the three-dimensional structure of voltage-gated potassium channels, *Trends Biochem. Sci. 24*, 345−349.
17. Kobertz, W. R., Williams, C., and Miller, C. (2000) Hanging gondola structure of the T1 domain in a voltage-gated K^+ channel, *Biochemistry 39*, 10347−10352.
18. Gulbis, J. M., Zhou, M., Mann, S., and MacKinnon, R. (2000) Structure of the cytoplasmic β subunit-T1 assembly of voltage-dependent K^+ channels, *Science 289*, 123−127.
19. Long, S. B., Campbell, E. B., and Mackinnon, R. (2005) Voltage sensor of Kv1.2: Structural basis of electromechanical coupling, *Science 309*, 897−903.
20. Antz, C., Geyer, M., Fakler, B., Schott, M. K., Guy, H. R., Frank, R., Ruppersberg, J. P., and Kalbitzer, H. R. (1997) NMR structure of inactivation gates from mammalian voltage-dependent potassium channels, *Nature 385*, 272−274.
21. Schott, M. K., Antz, C., Frank, R., Ruppersberg, J. P., and Kalbitzer, H. R. (1998) Structure of the inactivating gate from the Shaker voltage gated K^+ channel analyzed by NMR spectroscopy, *Eur. Biophys. J. 27*, 99−104.
22. Pervushin, K., Riek, R., Wider, G., and Wüthrich, K. (1997) Attenuated T2 relaxation by mutual cancellation of dipole−dipole coupling and chemical shift anisotropy indicates an avenue to NMR structures of very large biological macromolecules in solution, *Proc. Natl. Acad. Sci. U.S.A. 94*, 12366−12371.
23. Marley, J., Lu, M., and Bracken, C. (2001) A method for efficient isotopic labeling of recombinant proteins, *J. Biomol. NMR 20*, 71−75.
24. LeMaster, D. M., and Richards, F. M. (1988) NMR sequential assignment of *Escherichia coli* thioredoxin utilizing random fractional deuteriation, *Biochemistry 27*, 142−150.

25. LeMaster, D. M., and Richards, F. M. (1985) ^{1}H-^{15}N heteronuclear NMR studies of *Escherichia coli* thioredoxin in samples isotopically labeled by residue type, *Biochemistry 24*, 7263−7268.
26. Salzmann, M., Pervushin, K., Wider, G., Senn, H., and Wüthrich, K. (1998) TROSY in triple-resonance experiments: New perspectives for sequential NMR assignment of large proteins, *Proc. Natl. Acad. Sci. U.S.A. 95*, 13585−13590.
27. Salzmann, M., Pervushin, K., Wider, G., Senn, H., and Wüthrich, K. (1999) [^{13}C]-constant-time [^{15}N,^{1}H]-TROSY-HNCA for sequential assignments of large proteins, *J. Biomol. NMR 14*, 85−88.
28. Salzmann, M., Wider, G., Pervushin, K., Senn, H., and Wüthrich, K. (1999) TROSY-type triple-resonance experiments for sequential NMR assignments of large proteins, *J. Am. Chem. Soc. 121*, 844−848.
29. Grzesiek, S., Anglister, J., Hao, R., and Bax, A. (1993) Carbon-13 line narrowing by deuterium decoupling in deuterium/carbon-13/nitrogen-15 enriched proteins. Application to triple resonance 4D connectivity of sequential amides, *J. Am. Chem. Soc*. *115*, 4369−4379.
30. Pervushin, K., Braun, D., Fernández, C., and Wüthrich, K. (2000) [^{15}N,^{1}H]/[^{13}C,^{1}H]-TROSY for simultaneous detection of backbone ^{15}N-^{1}H, aromatic ^{13}C-^{1}H, and side-chain ^{15}N-^{1}H2 correlations in large proteins, *J. Biomol. NMR 17*, 195−202.
31. Zhu, G., Xia, Y. L., Nicholson, L. K., and Sze, K. H. (2000) Protein dynamics measurements by TROSY-based NMR experiments, *J. Magn. Reson. 143*, 423−426.
32. Pervushin, K., Wider, G., and Wüthrich, K. (1998) Single transition-to-single transition polarization transfer (ST2-PT) in [^{15}N,^{1}H]-TROSY, *J. Biomol. NMR 12*, 345−348.
33. Güntert, P., Dötsch, V., Wider, G., and Wüthrich, K. (1992) Processing of multidimensional NMR data with the new software PROSA, *J. Biomol. NMR 2*, 619−629.
34. Bartels, C., Xia, T. H., Billeter, M., Güntert, P., and Wüthrich, K. (1995) The program XEASY for computer-supported NMR spectral analysis of biological macromolecules, *J. Biomol. NMR 6*, 1−10.
35. Markley, J. L., Bax, A., Arata, Y., Hilbers, C. W., Kaptein, R., Sykes, B. D., Wright, P. E., and Wüthrich, K. (1998) Recommendations for the presentation of NMR structures of proteins and nucleic acids. IUPAC−IUBMB−IUPAB Inter-Union Task Group on the Standardization of Data Bases of Protein and Nucleic Acid Structures Determined by NMR Spectroscopy, *J. Biomol. NMR 12*, 1−23.
36. Battiste, J. L., and Wagner, G. (2000) Utilization of site-directed spin labeling and high-resolution heteronuclear nuclear magnetic resonance for global fold determination of large proteins with limited nuclear overhauser effect data, *Biochemistry 39*, 5355−5365.
37. Kosen, P. A. (1989) Spin labeling of proteins, *Methods Enzymol. 177*, 86−121.
38. Isacoff, E. Y., Jan, Y. N., and Jan, L. Y. (1991) Putative receptor for the cytoplasmic inactivation gate in the Shaker K^{+} channel, *Nature 353*, 86−90.
39. Jiang, Y., Lee, A., Chen, J., Ruta, V., Cadene, M., Chait, B. T., and MacKinnon, R. (2003) X-ray structure of a voltage-dependent K^{+} channel, *Nature 423*, 33−41.

BI0516430